Deep level transient spectroscopy study of heavy ion implantation induced defects in silicon

C. T.-K. Lew,[1,2,a] B. C. Johnson,[1,2] and J. C. McCallum[2]
[1]*Centre for Quantum Computing and Communication Technology, School of Physics, University of Melbourne, Melbourne, Victoria 3010, Australia*
[2]*School of Physics, University of Melbourne, Melbourne, Victoria 3010, Australia*

(Received 8 July 2018; accepted 5 September 2018; published online 25 September 2018)

Defects introduced by low fluence arsenic, antimony, erbium, and bismuth ion implantation have been investigated as a function of annealing temperature using deep level transient spectroscopy (DLTS) and Laplace-DLTS. The defects produced by heavy ion implantation are stable up to higher temperatures than those introduced by electron irradiation and low mass ions. This result is attributed to the enhanced defect interactions that take place in the dense collision cascades created by heavy ion implantation. As a consequence, broadened DLTS features are apparent, especially after annealing. Using high energy resolution Laplace-DLTS, the well-known singly charged divacancy and vacancy-donor pair are accompanied by additional apparent defect signals. This shows that Laplace-DLTS is highly sensitive to the type of damage present, and extreme care must be exercised for reliable Arrhenius analysis. *Published by AIP Publishing.* https://doi.org/10.1063/1.5047534

I. INTRODUCTION

Recent developments in quantum computing and the demonstrated suitability of ion implantation technologies for quantum-device fabrication[1–8] have highlighted the need for more detailed implantation-induced damage studies. Defect evolution upon thermal annealing after ion implantation is an extremely complex process, where implantation parameters such as ion mass, energy, and fluence can have a profound effect on the evolution of implantation-induced damage during subsequent annealing. Phosphorus is a common dopant used for quantum information processing applications at low concentrations.[1] However, interest is growing in the use of heavier ions, such as arsenic,[2,3] antimony,[5] erbium,[6] and bismuth[8,9], due to their unique spin properties. Electrically active defects in fully fabricated quantum information-related nano-scale devices can have a significant impact on normal device operation[2] by acting as sources of charge and spin noise. Both can affect the decoherence times of the foreign atom spin centers,[5] which is especially important in devices where the thermal budget might be limited.[6]

In the low fluence regime ($< 10^{12}\,\mathrm{cm}^{-2}$) of interest for single spin implantation[10] and in the case of light ions such as phosphorus, sparse mobile interstitials and vacancies generated by implantation are able to recombine with each other at room temperature. The Frenkel defect pairs that escape recombination (2%–4% for self implanted silicon at low doses)[11,12] may go on to form stable defect clusters or point defect pairs involving impurities (C, O) and dopant atoms (commonly B or P). Upon annealing, all simple point defect pairs anneal out by 350 °C.[11,12] For heavier ions, however, the dense collision cascades produce highly disordered zones and sometimes amorphous regions surrounding the ion track, favoring more complex defect interactions and clustering. The properties of simple point defects can show great variability as a result of strain arising from these dense collision cascade.[13–17] Their thermal stability and therefore their possible impact on quantum computer-related devices are not known.

In this work, we investigate the defects introduced by arsenic (As), antimony (Sb), erbium (Er), and bismuth (Bi) implantation in n-type silicon and monitor their thermal stability using DLTS[18] and Laplace-DLTS.[19] The latter technique was used to deconvolute usually unresolvable DLTS signals, especially weak signals that persist after high temperature anneals. Vacancy-related point defects were detected after implantation and are found not to anneal out until above 500 °C. This annealing temperature is significantly higher than that previously identified and is attributed to the type of damage formed by the heavy ion species used. In addition, minority carrier traps and the effects of inhomogeneous strain induced by heavy ion implantation particularly in relation to the application of Laplace-DLTS are explored.

II. EXPERIMENT

Czochralski-grown (Cz) n-type, P doped silicon with a resistivity of 0.8–0.9 Ω cm was implanted with As, Sb, Er, or Bi at room temperature to a fluence of $1 \times 10^{11}\,\mathrm{cm}^{-2}$. The implantation energies were chosen based on TRIM[20] simulations to place the implant peak at a depth of approximately 0.59 μm, equating to 0.9, 1.3, 2.0, and 2.5 MeV for As, Sb, Er, and Bi, respectively. This allowed us to electrically access the implant range using moderate reverse biases without substantial reverse bias leakage currents. Subsequent rapid thermal anneals were carried out in an argon atmosphere for 15 min at temperature increments of 100 °C. Front Au Schottky barrier diodes (SBDs) were thermally deposited through a shadow mask under vacuum, and InGa eutectic was applied to the back to form a back Ohmic contact.

[a]lewc@student.unimelb.edu.au

DLTS and Laplace-DLTS were carried out using a custom-built DLTS spectrometer consisting of a 1 MHz Boonton 7200 capacitance meter and an Agilent 33210A arbitrary waveform generator. Temperature scans ranged from 90 to 300 K in 2 K increments for conventional DLTS and raw transients were recorded using a 16 bit analog-to-digital (A/D) converter at a 2 MHz sampling rate. Signal averaging was employed for both DLTS and Laplace-DLTS up to $N = 60$ and $N = 2000$ transients per temperature increment, respectively. This was performed to improve the signal-to-noise ratio (SNR) by a factor proportional to $\sqrt{N}$ based on Poissonian statistics. The averaged transients were then treated with a running average algorithm to further increase the SNR and reduce the number of data points. Finally, the transients were analyzed with the double boxcar method[18] for conventional DLTS and the program package CONTIN[21] making use of the Tikhonov regularisation method for Laplace-DLTS.

For the measurements presented below, a $t_p = 40$ ms filling pulse with a quiescent reverse bias of $V_r = -2.0$ V and a filling pulse height of $V_p = 2.0$ V were used unless otherwise stated. The chosen parameters ensured that all traps were filled during the filling pulse, and the implant peak was probed. In addition, all DLTS spectra presented are displayed below using an emission rate of $e_n(T_{peak}) = 446.8$ Hz ($t_1 = 1.35$ ms and $t_2 = 3.45$ ms).

III. RESULTS AND DISCUSSION

Figure 1 shows the unannealed DLTS spectra for As, Sb, Er, and Bi implanted samples. We have adopted the convention where a positive DLTS peak corresponds to a majority charge carrier trap. For the unannealed samples, the observed peaks are the characteristic DLTS peaks attributed to the vacancy-oxygen pair (VO) at 0.16–0.18 eV below the conduction band (E_c), the doubly charged divacancy (V_2^{2-}) at 0.21–0.23 eV below E_c, and a convolution of the vacancy-phosphorus pair (VP) and the singly charged divacancy (V_2^-)

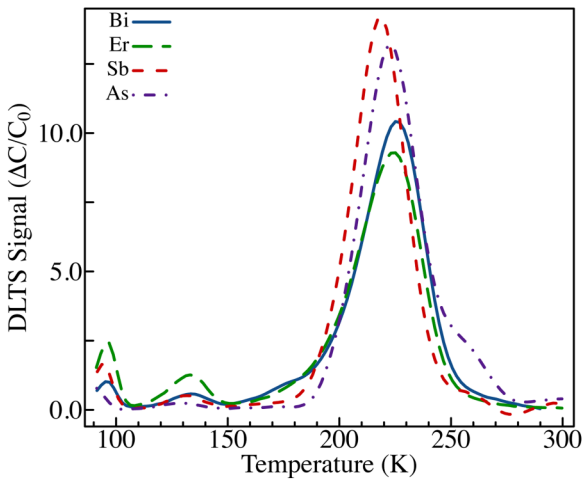

FIG. 1. DLTS spectra of unannealed As, Sb, Er, and Bi implanted samples. The characteristic DLTS peaks attributed to VO, V_2^{2-}, and a convolution of VP and V_2^- are present for all implanted ion species. However, shoulder peaks to the side of the prominent 220 K DLTS peak were observed and were found to be dependent on the implanted ion species.

at 0.42–0.45 eV below E_c. These values are from DLTS data of electron irradiated and light ion implanted samples in the low fluence regime.[11,12,16,17,22,23] Extreme care was exercised when directly comparing results with other published data, as it is known small variations in the calculated trap activation energies and capture cross sections can arise from variations in processing conditions and the broadening of DLTS signals caused by heavy ion implantation, which will be discussed further below. We found the trap activation energy for V_2^{2-} ranged from 0.22 to 0.25 eV below E_c and 0.40 to 0.44 eV below E_c for the VP/V_2^- peak in the unannealed samples implanted with As, Sb, Er, and Bi even though all other conditions were kept constant. Figure 2 shows the DLTS spectra for Sb implanted samples with and without various annealing treatments. Spectra for samples implanted with As, Er, and Bi are included in the supplementary material for completeness.

A peak situated at approximately 250 K in Fig. 2(a) appears as a shoulder peak to the right of the VP/V_2^- DLTS peak in the case of As and Sb implanted samples. A similar shoulder peak has been measured previously in plastically deformed silicon.[24] We note that this peak was not observed

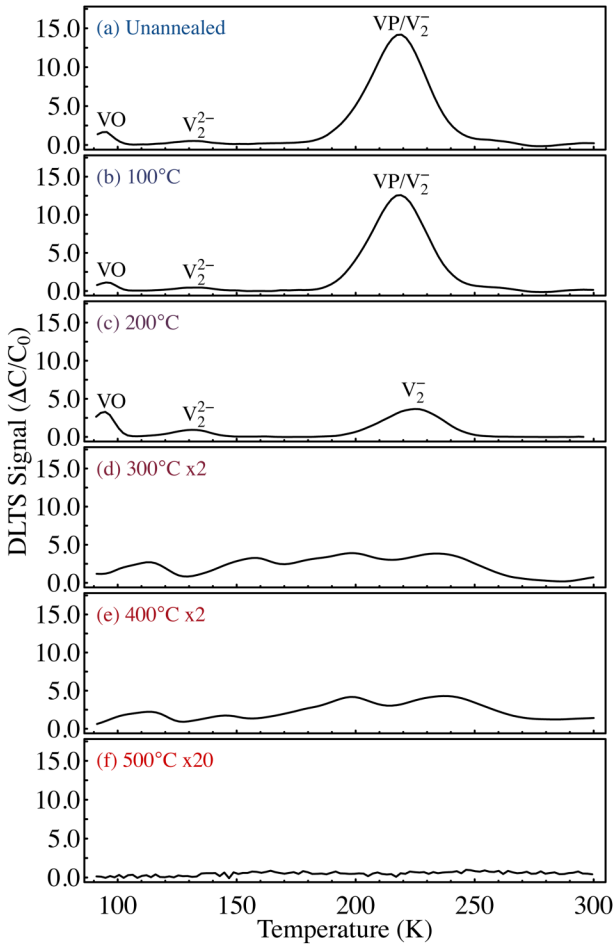

FIG. 2. DLTS spectra of 1.3 MeV antimony implanted silicon to a fluence of 1×10^{11} Sb/cm^2 prior and after isochronal annealing for 15 min. The major features are labeled with their corresponding atomic identity following convention up to 200 °C anneal. The spectra for samples annealed at 300 °C and above are multiplied by the factor indicated to highlight the weaker defect signals.

for the Er and Bi implanted samples. Instead, a shoulder peak to the left of the VP/V_2^- DLTS peak was observed. The presence and absence of the different shoulder peaks described are particularly evident in Fig. 1.

Figure 3(a) shows the Laplace-DLTS spectra for the unannealed Sb implanted sample measured in the temperature range between 196 and 232 K in 1 K increments to resolve the individual contributions of the VP/V_2^- DLTS peak. As expected, two prominent signals can be resolved with trap energies $E_c - E_T = 0.408 \pm 0.019$ and 0.416 ± 0.024 eV as calculated in the Arrhenius plot in Fig. 3(b) constructed from these signals. These originate from the VP and V_2^- defects, respectively, based on comparison of the results from the fits in Fig. 3(b) with literature values[11,12] and the small contribution of E1 with respect to E2 (~7% determined from the integrated area of the Laplace signal). Two smaller features can also be resolved; however, these display non-physical trap energies (i.e., trap energies greater than half of the bandgap) and are thought to be artefacts originating from the inverse Laplace transform algorithm. By presenting the Laplace spectra in this way, the difference between real signals and artefacts becomes more apparent. Similar results were obtained for the As implanted sample (not shown).

A. Inhomogeneous strain effects

For the two heavier ions, Er and Bi, the Laplace-DLTS spectra were much more complicated, which prevented the application of a standard Arrhenius analysis. As an example, Fig. 4(a) shows the Laplace spectra of the unannealed Er implanted sample, revealing multiple emission rates deviating from the expected VP and V_2^- signals shown in Fig. 3(a). Similar Laplace-DLTS data have been reported previously.[25,26] We suspect that this deviation is a result of localised inhomogeneous strain induced by heavy ion implantation rather than any shortcoming of the Laplace algorithm. Such strain may be expected from the greater excess vacancy concentration generated by Er and the denser damage cascades (TRIM simulation given in Fig. S4 of the supplementary material). Conventional DLTS do not show such dramatic effects in the presence of strain. Any physical broadening mechanisms such as inhomogeneous strain or localised disorder within the sample will also result in the broadening of the defect emission rates extracted from Laplace-DLTS.[27] It was previously demonstrated that the application of controlled uniaxial stress on defects with well-defined configurations with respect to the stress direction can be utilised to induce emission rate splittings that can be correlated to the spatial symmetry of the defect.[28] Together, it is reasonable to assume that inhomogeneous strain caused by heavy ion implantation gives rise to a random distribution of both the broadening and splitting of emission rates, making the interpretation of the Laplace-DLTS spectra for an ensemble of multiple defects extremely difficult.

Furthermore, we find that the Laplace-DLTS spectra are very sensitive to the probed depth in Er and Bi implanted samples. The positions, width, and number of Laplace peaks can vary significantly with biasing conditions as different depth regions containing a different strain and defect distribution are probed. By viewing individual Laplace-DLTS spectrum over a broad temperature range, the effects of strain induced emission rate splitting are clear, as seen in Fig. 4(a). We find that the emission rate splitting is much less prominent near the end of range of the implant in the interstitial rich region as indicated in Fig. 4(b). The effect of inhomogeneous broadening on the Laplace data makes interpretation difficult, and assignment of these peaks to additional defects as suggested previously[25,26] cannot be entirely justified.

B. Annealing trends

Upon annealing at 100 °C, the DLTS peak heights of VO, V_2^{2-}, and VP/V_2^- decrease as expected [Fig. 2(b)]. The VP/V_2^- DLTS peak height continues to decrease after annealing at 200 °C, but both VO and V_2^{2-} concentrations increase regardless of implanted ion species. The reverse annealing behavior of VO was previously suggested to be due to the migration of VP upon annealing and subsequently being captured by existing P^+ ion to form VP_2, which has a DLTS signal that overlaps with the VO peak.[15,29] The doubly charged divacancy is known to have a strong dependence on strain. Svensson *et al.*[16,17] have previously suggested that V_2^{2-} is more strongly affected by the strain induced inhibition of the Jahn-Teller bond reordering, accounting for the dramatic difference between the concentrations of V_2^{2-} and V_2^- in heavy ion implanted samples as seen in our data in Fig. 2(a). The ratio between the doubly and singly charged divacancy varied between 0.02 and 0.06

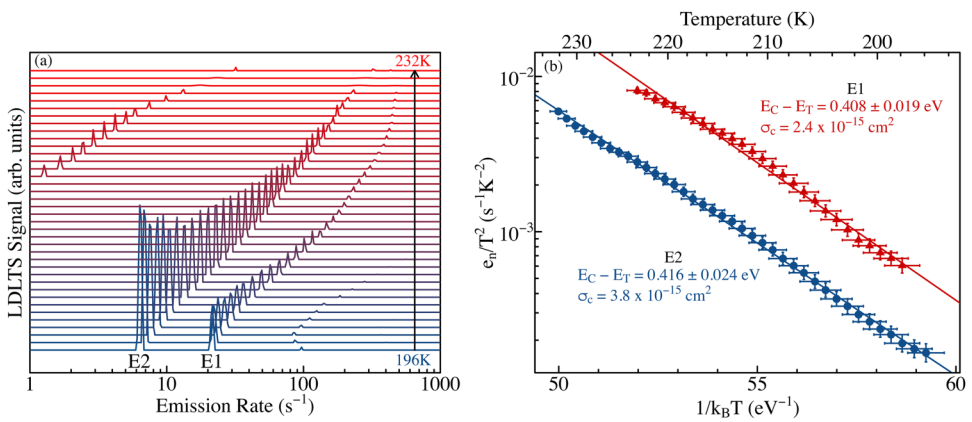

FIG. 3. (a) Individual Laplace-DLTS spectrum for the unannealed Sb sample plotted as a function of temperature offset vertically for clarity. (b) Arrhenius plot for E1 and E2 observed in (a). Non-physical trap parameters were found for the other two resolved emission rates and are thought to arise from mathematical artefacts resulting from the inverse Laplace transform algorithm. Solid lines are linear fits to the data.

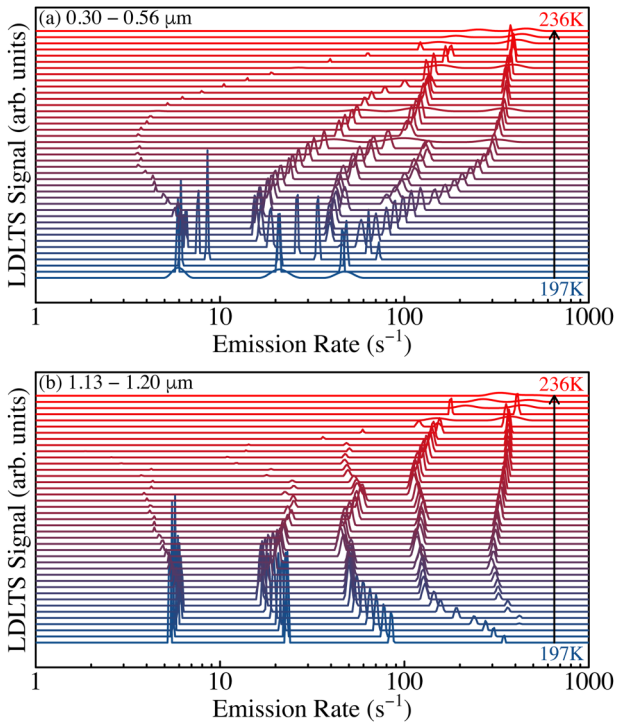

FIG. 4. Individual Laplace DLTS spectrum for the unannealed Er sample shifted vertically as a function of temperature probing either the (a) vacancy rich region ($V_r = -2$ V, $V_p = 2$ V) or the (b) interstitial rich region ($V_r = -8$ V, $V_p = 2$ V).

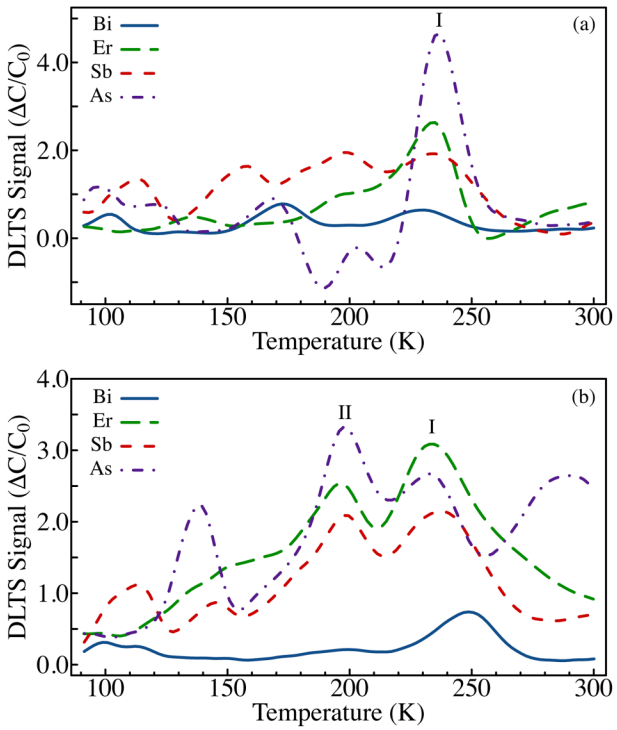

FIG. 5. DLTS spectra of As, Sb, Er, and Bi implanted samples annealed at (a) 300 °C and (b) 400 °C. The presence of a specific DLTS feature appears to have a dependence on the implanted ion species, but all spectra in (a) contain the same peak located at 240 K (labeled I) and all spectra in (b) contain an additional peak located at 200 K (labeled II).

for the ion species used in this work. A relationship between $[V_2^{2-}]/[V_2^-]$ and the mass of the implanted ion species as previously suggested[30] cannot be established, possibly due to the low SNR of the $[V_2^{2-}]$ signal approaching our estimated detection limit and the extremely heavy ion masses used in this study. The reverse annealing behavior of V_2^{2-} has been previously assigned to the alleviation of strain induced by ion implantation responsible for the deviation from $[V_2^{2-}]/[V_2^-] \approx 1$ observed in electron irradiated samples.[15–17,23,31] The ratio between the different charge states of the divacancy increases to 0.15–0.23 after a 200 °C anneal, suggesting that not all strain is alleviated in our heavy ion implanted samples.

Regardless of implanted ion species, the DLTS spectra undergo a dramatic transition when annealed above 300 °C as seen in Fig. 5(a). At this annealing temperature, the presence of specific peaks and features appears to become dependent on the implanted ion species. However, one feature located at approximately 240 K [I in Fig. 5(a)] is seen for all implanted ion species and is believed to be due to the presence of V_2O^- from the capture of mobile V_2^- by electrically inactive interstitial O.[32] Similar to its precursor, the divacancy-oxygen defect complex forms two charge states located at E_c −0.21 eV and E_c −0.47 eV, respectively. This corresponds to a DLTS peak that appears at a lower and higher temperature than its V_2^{2-} and V_2^- precursors, respectively. Indeed, a DLTS peak situated at a slightly higher temperature with respect to V_2^{2-} was observed in Figs. 2(c) and 2(d); however, the presence of its counterpart in proximity to the V_2^{2-} peak is not discernible. We note that V_2O^- persists after a 400 °C anneal and exhibits a reverse annealing behavior as seen in Fig. 6 except for the As implanted sample, possibly due to a compensation effect from the negative DLTS peaks observed in Fig. 5(a). After a 400 °C anneal as shown in Fig. 5(b), a temperature that is often quoted as being sufficient to remove vacancy-related defects in silicon,[11,12] DLTS features were still clearly present. An additional feature located at approximately 200 K [II in Fig. 5(b)] appears in all DLTS spectra regardless of implanted ion species and is believed to be due to the formation of the L-center previously proposed to consist of a trivacancy-oxygen complex (V_3O) situated at E_c −0.36 eV.[22,33] The other additional peaks observed in Fig. 5 are believed to be related to the formation of vacancy-related clusters. Implementation of the lock-in weighting function with a higher SNR[34] and the Gaver-Stehfest (GS4)[35] weighting function with a higher energy resolution revealed similar spectra (not shown), suggesting the broadness of the spectra is not due to the convolution of multiple defect species. Furthermore, at this annealing temperature and implantation fluence, the formation of extended defects such as dislocations that also have broad DLTS features[36,37] or implanted ion species related defect structures is not expected. The energy levels associated with these features were difficult to determine due to the fact that they are not clearly resolved and the poor SNR resulting from the small defect signal amplitude after annealing.

A 500 °C anneal was required to remove all DLTS peaks observed originally in the unannealed samples. As can be seen in Fig. 2(f), a broad featureless signal still remains even after a 500 °C anneal. This signal is especially apparent for

the Bi implanted sample [see Fig. S3(f) in the supplementary material] and is thought to arise from extended defects, which introduce a broad density of states into the bandgap. Higher temperature anneals were performed for the As implanted sample, and it was observed that a 600 °C anneal was required to remove all DLTS peaks. The higher annealing temperature required to remove vacancy-related defects introduced by low fluence heavy ion implantation is highlighted in Fig. 6 by following the broad annealing behavior of the prominent 220 K DLTS peak and comparing it with data extracted from the literature for a light ion, low fluence implanted sample[30] in which a sharp contrast of the annealing behavior can be observed.

C. Minority charge carrier defects

Minority charge carrier traps appearing as negative DLTS peaks following the convention we have adopted were observed in the 200 °C and 300 °C annealed As implanted samples as shown in Fig. 7. This is not expected when only reverse bias and majority charge carrier injection pulses are used. However, the observation of a reverse sign DLTS signal in SBDs has been previously reported by various groups, alluding to poor non-ideal back Ohmic contact[38,39] or the injection of minority charge carriers under reverse bias using an ultrahigh barrier height.[40–42] We consider these two possibilities as follows.

Firstly, we rule out the likelihood of a poor back Ohmic contact. Generally, such a contact can be modelled as a large resistor in series with the SBD. Most capacitance meters record the capacitance of an equivalent parallel circuit with a capacitive C_p and resistive R_p term, rather than an equivalent series circuit. When the series resistance R_s is finitely large (i.e., non-ideal back Ohmic contact), the sign of the measured capacitance can sometimes be reversed when the capacitance of an equivalent parallel circuit is measured.[38–40] The capacitance difference measured in a double boxcar DLTS measurement can be expressed as[43]

$$\Delta C_m = \frac{\Delta C}{1+(2\pi f r_s C)^2}\left(1-\frac{2(2\pi f r_s C)^2}{1+(2\pi f r_s C)^2}\right), \quad (1)$$

where ΔC_m is the measured capacitance difference, ΔC is the actual capacitance difference, f is the AC test signal frequency of the capacitance meter, r_s is the series resistance, and C is the quiescent capacitance. Substituting the appropriate values into Eq. (1) with the quiescent capacitance ranging from 53.1 to 73.7 pF in the temperature range between 90 and 300 K and $f = 1$ MHz, ΔC_m is expected to change signs when $r_s \gtrsim 3\,\text{k}\Omega$. We inserted an external 3 kΩ resistor in series with the sample and saw that the addition of the external resistor was able to flip the sign of the transient. Therefore, this suggests the series resistance of the back contact is sufficiently small such that the back contact cannot be considered non-ideal, and we conclude the observed negative DLTS signal was not due to a non-ideal back contact. It was further supposed that a filling pulse to 0 V near forward bias may result in minority charge carrier injection. However, when pulsing from $V_r = -5$ V instead of $V_r = -2$ V with the same filling pulse height of $V_p = 2.0$ V, a similar DLTS spectrum was obtained with smaller peak amplitudes (not shown), but the negative DLTS peaks persisted.

Stolt and Bohlin[42] have previously demonstrated the detection of minority charge carrier traps using an ultrahigh Schottky barrier height ($\phi_{Bn} \sim 0.9$ eV) under reverse bias in DLTS where an inversion layer near the metal-semiconductor

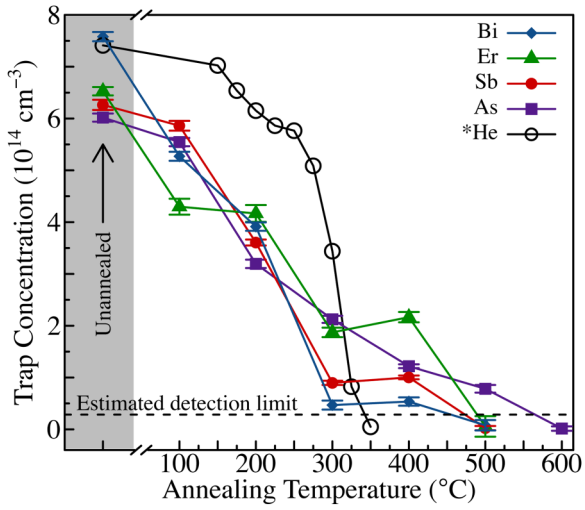

FIG. 6. Trap concentration of the prominent 220 K DLTS peak produced from various heavy ion implanted species as a function of annealing temperature. Sample annealing data of the 220 K DLTS peak in a He implanted sample is plotted for comparison.[30] The trap concentration was calculated from experimentally found carrier concentration for each sample instead of the sample resistivity.

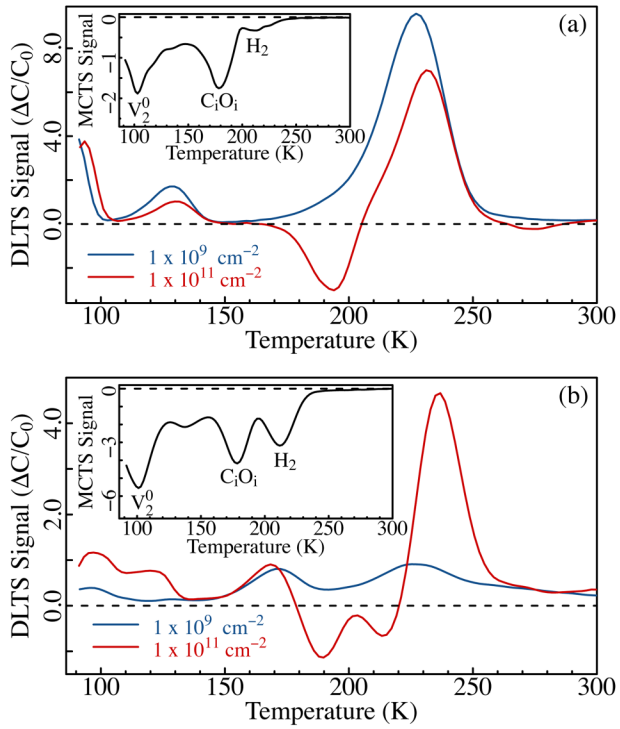

FIG. 7. DLTS spectra of (a) 200 °C and (b) 300 °C annealed As implanted samples to a fluence of 1×10^9 cm^{-2} (blue solid lines) and 1×10^{11} cm^{-2} (red solid lines). The insets show MCTS performed on the 1×10^{11} cm^{-2} fluence samples exhibiting negative DLTS peaks, revealing multiple minority carrier trap peaks. Their atomic origins are labeled following convention.

interface could form. The inversion layer acts as a readily available source of minority charge carriers (i.e., holes) in which minority charge carrier traps are now also able to participate in the trapping and emission process in response to a voltage pulse under reverse biases. For the samples that exhibited a negative DLTS signal, the barrier heights were determined experimentally from I−V characteristics in forward biases greater than $V > 3k_BT/q$ according to thermionic-emission theory[44]

$$\phi_{Bn} = \frac{k_B T}{q} \ln\left(\frac{A^{\star\star} T^2}{J_0}\right), \tag{2}$$

where k_B is Boltzmann's constant, q is the electron charge, T is the temperature, $A^{\star\star}$ is the Richardson constant equal to 120 A cm^{-2}K^{-2}, and J_0 is the extrapolated saturation current density at 0 V. The barrier heights were experimentally found to be 0.83 and 0.87 eV for the 200 °C and 300 °C annealed As implanted samples, respectively. An additional set of samples implanted at a lower fluence of 1×10^9 cm^{-2} with the same annealing conditions were measured using DLTS (blue solid lines in Fig. 7) and show only positive DLTS signals as expected. The barrier heights calculated from Eq. (1) were found to be 0.73 and 0.78 eV for the 200 °C and 300 °C annealed low fluence As implanted samples, respectively. The slight increase in the barrier height with fluence may be related to the compensating traps in the damage layer.[36,37]

Minority carrier transient spectroscopy (MCTS) was performed by deliberately injecting minority charge carriers into the samples using an above bandgap 940 nm high speed infrared emitting diode to confirm that the negative DLTS peaks were reproducible. In the insets of Fig. 7, MCTS data reveal multiple negative peaks, showing striking resemblance to the negative DLTS features observed. An additional MCTS peak at 100 K was observed; however, it is absent in the conventional DLTS spectra. Good agreement between the major features observed in the MCTS spectra and DLTS spectra observed for p-type electron irradiated[12] and light ion implanted[11,12] silicon annealed in the temperature range between 200 °C and 300 °C allowed for the identification of the atomic origins of the MCTS peaks. The observed MCTS peaks are attributed to the neutrally charged divacancy (V_2^0), the carbon-oxygen interstitial complex (C_iO_i), and an interstitial type defect labeled H_2 following convention.[11,12]

IV. CONCLUSION

The annealing behavior of defects introduced by heavy ion implantation of As, Sb, Er, and Bi is shown to persist up to temperatures significantly higher than what has been previously observed for electron irradiation and light ion, low fluence implantation. This is a consequence of the dense damage cascades formed during heavy ion implantation. The role of implantation induced strain resulting from the highly disordered collision cascades formed during implantation are also observed to significantly affect the properties of the defect emission rate in transient based defect spectroscopy. The DLTS spectra up to 200 °C anneal are well characterised and are in reasonable agreement with previous studies. However, at higher annealing temperatures, between 300 °C and 400 °C, an apparent dependence on the implanted ion species is observed as a direct result of enhanced defect interactions caused by heavy ion implantation.

The annealing strategies required to fabricate device that makes use of the unique spin properties of these heavy ions will certainly require a thermal budget at least above 500 °C for samples implanted with Sb, Er, and Bi and at least above 600 °C for samples implanted with As for 15 min to remove the majority of all intrinsic vacancy-related defects produced during heavy ion implantation. Studies on more complex quantum computing related test device structures that include an oxide and its effectiveness in response to thermal annealing required for damage repair are currently under progress.

SUPPLEMENTARY MATERIAL

See supplementary material for the complete set of DLTS spectra prior and after various annealing treatments and the full TRIM simulation for samples implanted with As, Er, and Bi.

ACKNOWLEDGMENTS

This research was funded by the Australian Research Council Centre of Excellence for Quantum Computation and Communication Technology (No. CE110001027). The authors acknowledge access to ion-implantation facilities at the ACT node of the Heavy-Ion-Accelerator Capability funded by the Australian Government under the NCRIS program.

[1]J. J. Pla, K. Y. Tan, J. P. Dehollain, W. H. Lim, J. J. L. Morton, D. N. Jamieson, A. S. Dzurak, and A. Morello, Nature **489**, 541 (2012).
[2]G. Lansbergen, R. Rahman, C. Wellard, I. Woo, J. Caro, N. Collaert, S. Biesemans, G. Klimeck, L. Hollenberg, and S. Rogge, Nat. Phys. **4**, 656 (2008).
[3]A. J. Sigillito, A. M. Tyryshkin, T. Schenkel, A. A. Houck, and S. A. Lyon, Nat. Nanotechnol. **12**, 958 (2017).
[4]A. M. Tyryshkin, S. Tojo, J. J. L. Morton, H. Riemann, N. V. Abrosimov, P. Becker, H.-J. Pohl, T. Schenkel, M. L. W. Thewalt, K. M. Itoh, and S. A. Lyon, Nat. Mater. **11**, 143 (2012).
[5]T. Schenkel, J. Liddle, A. Persaud, A. Tyryshkin, S. Lyon, R. De Sousa, K. B. Whaley, J. Bokor, J. Shangkuan, and I. Chakarov, Appl. Phys. Lett. **88**, 112101 (2006).
[6]C. Yin, M. Rancic, G. G. de Boo, N. Stavrias, J. C. McCallum, M. J. Sellars, and S. Rogge, Nature **497**, 91 (2013).
[7]L. Robledo, L. Childress, H. Bernien, B. Hensen, P. F. A. Alkemade, and R. Hanson, Nature **477**, 574 (2011).
[8]J. Pla, A. Bienfait, G. Pica, J. Mansir, F. Mohiyaddin, Z. Zeng, Y.-M. Niquet, A. Morello, T. Schenkel, J. Morton *et al.*, Phys. Rev. Appl. **9**, 044014 (2018).
[9]G. Wolfowicz, A. M. Tyryshkin, R. E. George, H. Riemann, N. V. Abrosimov, P. Becker, H.-J. Pohl, M. L. W. Thewalt, S. A. Lyon, and J. J. L. Morton, Nat. Nanotechnol. **8**, 561 (2013).
[10]T. Schenkel, C. Lo, C. Weis, A. Schuh, A. Persaud, and J. Bokor, Nucl. Instr. Meth. B **267**, 2563 (2009).
[11]S. Libertino, J. Benton, D. Jacobson, D. Eaglesham, J. Poate, S. Coffa, P. Kringhøj, P. Fuochi, and M. Lavalle, Appl. Phys. Lett. **71**, 389 (1997).
[12]J. L. Benton, S. Libertino, P. Kringhøj, D. J. Eaglesham, J. M. Poate, and S. Coffa, J. Appl. Phys. **82**, 120 (1997).
[13]R. M. Fleming, C. Seager, D. Lang, P. Cooper, E. Bielejec, and J. Campbell, J. Appl. Phys. **102**, 043711 (2007).
[14]R. M. Fleming, C. Seager, D. Lang, E. Bielejec, and J. Campbell, J. Appl. Phys. **104**, 083702 (2008).
[15]R. M. Fleming, C. Seager, E. Bielejec, G. Vizkelethy, D. Lang, and J. Campbell, J. Appl. Phys. **107**, 053712 (2010).
[16]B. G. Svensson, B. Mohadjeri, A. Hallén, J. H. Svensson, and J. W. Corbett, Phys. Rev. B **43**, 2292 (1991).

[17]B. G. Svensson, C. Jagadish, A. Hallen, and J. Lalita, Phys. Rev. B **55**, 10498 (1997).
[18]D. V. Lang, J. Appl. Phys. **45**, 3023 (1974).
[19]L. Dobaczewski, A. R. Peaker, and K. B. Nielsen, J. Appl. Phys. **96**, 4689 (2004).
[20]J. F. Ziegler, M. D. Ziegler, and J. P. Biersack, Nucl. Instr. Meth. B **268**, 1818 (2010).
[21]S. W. Provencher, Comp. Phys. Commun. **27**, 229 (1982).
[22]M. Mikelsen, J. H. Bleka, J. S. Christensen, E. V. Monakhov, B. G. Svensson, J. Härkönen, and B. S. Avset, Phys. Rev. B **75**, 155202 (2007).
[23]P. Pellegrino, P. Lévêque, J. Lalita, A. Hallén, C. Jagadish, and B. G. Svensson, Phys. Rev. B **64**, 195211 (2001).
[24]D. Cavalcoli, A. Cavallini, and E. Gombia, Phys. Rev. B **56**, 10208 (1997).
[25]J. Evans-Freeman, N. Abdelgader, P. Kan, and A. Peaker, Nucl. Instr. Meth. B **186**, 41 (2002).
[26]N. Abdelgader and J. Evans-Freeman, J. Appl. Phys. **93**, 5118 (2003).
[27]A. Peaker, J. Evans-Freeman, P. Kan, I. Hawkins, J. Terry, C. Jeynes, and L. Rubaldo, Mater. Sci. Eng. B **71**, 143 (2000).
[28]O. Andersen, L. Dobaczewski, A. Peaker, K. B. Nielsen, B. Hourahine, R. Jones, P. Briddon, and S. Öberg, Physica B **308**, 139 (2001).
[29]A. N. Larsen, C. Christensen, and J. W. Petersen, J. Appl. Phys. **86**, 4861 (1999).
[30]L. Vines, E. Monakhov, J. Jensen, A. Y. Kuznetsov, and B. Svensson, Phys. Rev. B **79**, 075206 (2009).
[31]E. Monakhov, J. Wong-Leung, A. Y. Kuznetsov, C. Jagadish, and B. G. Svensson, Phys. Rev. B **65**, 245201 (2002).
[32]V. Markevich, A. Peaker, S. Lastovskii, L. Murin, and J. Lindström, J. Phys. Condens. Matter **15**, S2779 (2003).
[33]M. Mikelsen, E. Monakhov, B. Avset, and B. Svensson, Phys. Scr. **2006**, 81 (2006).
[34]C. Crowell and S. Alipanahi, Solid-State Electron. **24**, 25 (1981).
[35]A. Istratov, J. Appl. Phys. **82**, 2965 (1997).
[36]P. Giri and Y. Mohapatra, J. Appl. Phys. **84**, 1901 (1998).
[37]P. Giri and Y. Mohapatra, Mater. Sci. Eng. B. **71**, 327 (2000).
[38]J. Lauwaert, S. Khelifi, K. Decock, M. Burgelman, and H. Vrielinck, J. Appl. Phys. **109**, 063721 (2011).
[39]A. Broniatowski, A. Blosse, P. Srivastava, and J. Bourgoin, J. Appl. Phys. **54**, 2907 (1983).
[40]S. Johnston, S. Kurtz, D. Friedman, A. Ptak, R. Ahrenkiel, and R. Crandall, Appl. Phys. Lett. **86**, 072109 (2005).
[41]F. Auret and M. Nel, J. Appl. Phys. **61**, 2546 (1987).
[42]L. Stolt and K. Bohlin, Solid-State Electron. **28**, 1215 (1985).
[43]P. Grillot, S. Ringel, E. Fitzgerald, G. Watson, and Y. Xie, J. Appl. Phys. **77**, 676 (1995).
[44]S. Sze and K. Ng, *Physics of Semiconductor Devices* (Wiley, 2006).